Available online at www.sciencedirect.com
ScienceDirect
Journal of the European Ceramic Society 29 (2009) 1029–1037
www.elsevier.com/locate/jeurceramsoc

Discrete element method (DEM) modeling of fracture and damage in the machining process of polycrystalline SiC

Yuanqiang Tan [a], Dongmin Yang [a], Yong Sheng [b,*]

[a] School of Mechanical Engineering, Xiangtan University, Hunan 411105, China
[b] School of Civil Engineering, University of Leeds, Leeds LS2 9JT, UK

Received 27 February 2008; received in revised form 23 July 2008; accepted 29 July 2008
Available online 11 September 2008

Abstract

Discrete element method (DEM) was employed in the research works presented in this paper to simulate the microscopic machining process of ceramics. A densely packed particle assembly system of the polycrystalline SiC has been generated in DEM software package PFC2D using bonded-particle model (BPM) in order to represent for the ceramic part numerically. Microscopic mechanical properties of SiC were calibrated by comparing the numerical tests in PFC2D with the equivalent experimental results, and introduced into the subsequent modeling of the ceramic machining process. The dynamic process of initiation and propagation of the micro-cracks under various machining conditions has been explicitly modeled in the DEM simulations. The numerical results from DEM modeling agreed well with the experimental observations and theoretical predictions. Rational relations between cracking damage of ceramics and cutting conditions have been established based on the analysis of simulation results. A generalized model of defining the range of inelastic zone has also been developed based on the numerical results. Moreover, this study has demonstrated the advantage of DEM model in its capability of revealing the mechanical details of machining process at micro-scale.
Crown Copyright © 2008 Published by Elsevier Ltd. All rights reserved.

Keywords: SiC; Mechanical properties; Microstructure; Fracture; Discrete element method

1. Introduction

Machining technologies of ceramics have been developed very fast over recent years due to the growing industrial demand of higher machining accuracy and better surface quality of ceramic elements. But the brittle nature of ceramics makes the machining process very difficult comparing to the ductile materials. Many experimental researches have been carried out to study the machining mechanism of ceramics in the mode of grinding,[1,2] scratching test[3,4] and single point diamond turning.[5,6] Furthermore, theoretical and numerical methods have also been developed to compliment the experimental researches, with the application of indentation fracture mechanics,[7] continuum damage mechanics[8] and finite element method.[9] Recently, the molecular dynamics (MD) method has been used to simulate the nano-machining process and analyze the machining mechanism of some monocrystalline materials at atom scale, e.g. copper,[10] germanium,[11] and silicon.[12,13]

During the machining process of ceramics, residual defects on the finished surface such as asperities and micro-cracks often appear. Even if the cutting depth is small enough for the plastic deformation to appear, the friction between the blunt tool and work piece may also lead to micro-cracks on the plastic surface.[14] This process is very difficult to be experimentally measured or theoretically analyzed, and also is almost impossible to be modeled by the molecular dynamics method due to the excessive computing costs. It is therefore essential to adopt alternative numerical approaches to study the initiation and propagation of micro-cracks during the machining process in order to improve our understanding of the mechanism of the machining process of ceramics.

Since the micro-structure of polycrystalline ceramics consist of crystal particles and pores, the ceramic bulk can be treated as an assemblage of discrete particles bonded together randomly. Furthermore the intergranular fracture of the ceramics can be naturally represented by the separation of particles due to breakage of bonds. This principle has been adopted in the particle

* Corresponding author. Tel.: +44 113 3433200; fax: +44 113 3432265.
E-mail address: y.sheng@leeds.ac.uk (Y. Sheng).

0955-2219/$ – see front matter. Crown Copyright © 2008 Published by Elsevier Ltd. All rights reserved.
doi:10.1016/j.jeurceramsoc.2008.07.060

Nomenclature

E_c	Young's modulus of the particles
$\overline{E_c}$	Young's modulus of the parallel-bond
k_n/k_s	ratio of normal to shear stiffness of the particles
$\overline{k_n}/\overline{k_s}$	ratio of normal to shear stiffness of the parallel-bond
R_{max}/R_{min}	ratio of particles' maximum radius to minimum radius

Greek symbols

$\bar{\lambda}$	radius multiplier of the parallel-bond
μ	friction factor
ρ	density of the particles
$\overline{\sigma_n}$	tensile strength of the parallel-bond
$\overline{\sigma_s}$	shear strength of the parallel-bond

discrete element method (DEM) in the simulations of rock[15,16] and other particulate materials.[17,18]

The aim of this study is to develop a DEM model of polycrystalline SiC to simulate the ceramics machining process so that a quantitative description of the cracks initiation and propagation can be obtained and used for the assessment of the machining techniques.

2. Discrete element method and bonded-particle model (BPM)

DEM was proposed by Cundall in the context of rock mechanics[19] and has been implemented in many other fields, such as geomaterials,[20] granular materials[21] and concrete.[22] The particle discrete element method assumes the particle elements are rigid spheroid or disc, and can overlap or detach. The contact forces between two particles are determined from the overlap and relative movements of the particle pair according to a specified force–displacement law.

DEM allows particles to be bonded together at contacts and to be separated under external forces. It can simulate the motion of individual particles and also the behavior of bulk material formed by assembling many particles through bonds at contacts. The later was defined as BPM.[24,25] In this study, the particle flow codes in two dimensions (PFC2D),[23] which is a program based on the principle of DEM, is used as the simulation platform. The assembly was made of microscopic particles which were considered as circular disks with unit thickness. Parallel bond model[26] was adopted in this study to simulate the bonds at contacts between particles. Through adjusting the particle sizes and the strengths of the parallel bond, PFC2D can simulate various mechanical behaviors of ceramics. The bonds between particles will break when the external loading exceeds the strength of bonds, and cracks will form directly between two particles.

In order to construct a DEM model in PFC2D which is similar to the micro-structure of ceramics, the material-genesis procedure was utilized to generate a dense packing of non-uniform-sized circular particles in two dimensions, as shown in Fig. 1. Details of the procedure were described elsewhere.[24,26]

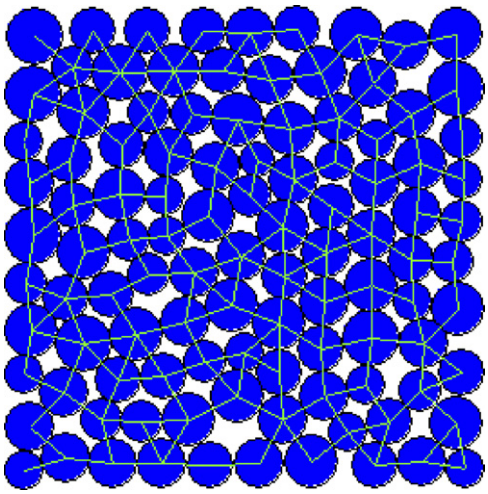

Fig. 1. Densely packed particle assembly in DEM.

3. Calibration of the DEM model for ceramics

The mechanical properties of ceramics are usually described by their elastic modulus, unconfined compressive strength, Poisson's ratio, tensile strength, bending strength and fracture toughness, etc. While in a DEM model, the properties of particles and the contacts between the particles need to be specified at micro-scale, e.g. particle stiffness, parallel bond strengths and the friction coefficient between particles. Since microscopic properties at particle level are very difficult to be determined by experimental measurements, it is essential to establish a correlation between the properties of the bulk materials and properties at the particle scale to validate the particle properties used in DEM modeling. This can be achieved by a calibration process suggested in PFC2D manuals.[26] In this paper, the unconfined compressive test, the Brazilian test, the three-point bending test and the fracture toughness test of SiC were carried out to calibrate the properties of particles and parallel bonds in BPM so that the particle assembly in DEM model can realistically represent for the mechanical behavior of ceramics in the subsequent modeling of the machining process.

3.1. Unconfined compressive test

Since the shear strength of the ceramics is usually much larger than the tensile strength, mode-I tensile cracks in forms of vertical and lateral cracks can be observed residing on the finished surface. The fracture toughness of ceramics has significant effect on the quality of finished surface. Potyondy and Cundall related the linear elastic fracture mechanics (LEFM) to the BPM, and proposed a useful formula[24]:

$$K_{Ic} = \beta\sigma_t'\sqrt{\pi\alpha R} \quad (1)$$

where α and β are dimensionless factors, σ_t' is the tensile strength of the parallel bond, R is the average radius of the particles.

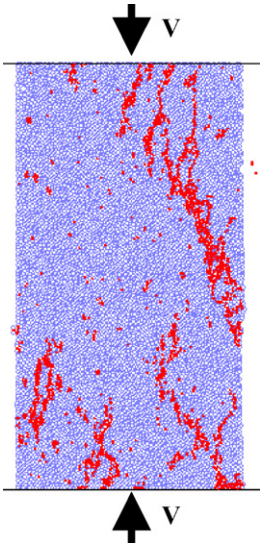

Fig. 2. Unconfined compressive test (cracks described by red/black lines). (For interpretation of the references to color in this figure legend, the reader is referred to the web version of the article.)

Note that the K_{IC} is related to the tensile strength of the parallel bond and the size of the particles. In order to match the K_{IC} of the particle assembly in DEM to the observed experimental value, the size distribution of the particles cannot be random, and should be determined according to Eq. (1).

In PFC2D, the unconfined compression test can be simplified to a model of two moving walls compressing the particles assembly, as illustrated in Fig. 2 with red dots indicating the break of bonds and where the micro-cracks can be found. The tested specimen of assembly is 0.8 mm in height, 0.4 mm in width and consists of 11,313 particles. The smallest size of the particles is 2.2 μm, the ratio of the largest in size to the smallest is set to 1.5. The porosity ratio is 0.16, which is a reasonable value for a dense packing.[27] The modulus E, Poisson's ratio ν and unconfined compression strength (UCS) of the SiC particle assembly can be obtained through the DEM simulation. Numerical results with the comparison of the experimental measurements are presented in Table 1.

Table 1
Main mechanical properties of SiC in macro-tests and in DEM

Mechanical properties	Experiment results[28,35]	DEM model results
Elastic modulus E (GPa)	420	429
Poisson's ratio ν	0.14	0.14
UCS σ_c (MPa)	2000	1996
Bending strength σ_{b3} (MPa)	500–800	656
Fracture toughness K_{IC} (MPa m$^{1/2}$)	3.5	3.5
Brazilian tensile strength σ_t (MPa)	214	387

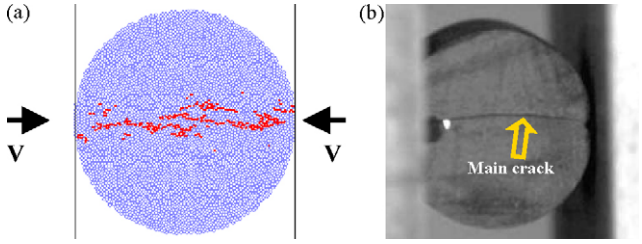

Fig. 3. Brazilian test. (a) DEM simulation result; (b) experimental snapshot of the main crack in Ref. [28].

3.2. Brazilian test

Brazilian test was used to calibrate the tensile strength of the specimen in DEM model. The diameter of the Brazilian disk used in the numerical tests is 0.4 mm in diameter, and is made of 4477 particles. The disk was crushed by the lateral walls moved towards each other with a low speed. The splitting plane is basically horizontal and it agrees well with the experimental observation,[28] which is depicted in Fig. 3. Note that the tensile strength of the SiC assembly in DEM model is a bit larger than experimental measurements.[28] This may due to the fact that Brazilian test results are very sensitive to size effect.[29]

3.3. Three-point bending test

Biaxial test is usually employed to obtain the shear strength and the strength envelope of rock.[24,26] For ceramics, shear strength is often much larger than tensile strength and therefore is regarded as less important in the development of fractures. In this research, the three-point bending test was adopted to evaluate the bending strength of ceramics, which can be easily converted to the shear strength. The numerical model was illustrated in Fig. 4, with dimensions of 1.0 mm in length and 0.2 mm in height. Two fixed balls were used to support the specimen. A rigid circular wall which is moving downward at a speed of 0.05 m/s was used to apply quasi-static load. The maximum force applied to cause the failure of the assembly is then used to calculate the bending strength. The fracture plane is clearly visible in the particle assembly, as is indicated by the red dots in Fig. 4.

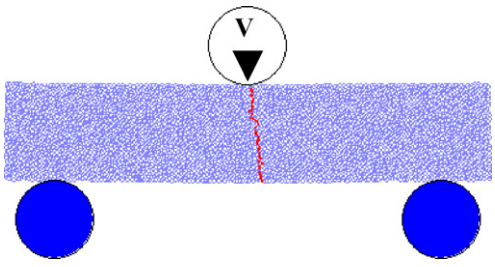

Fig. 4. Three-point bending test. (For interpretation of the references to color in the text, the reader is referred to the web version of the article.)

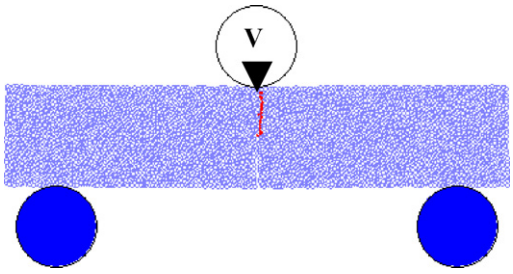

Fig. 5. SENB test.

3.4. Fracture toughness test

In order to calibrate the fracture toughness of SiC assembly, a single-edge notch bending (SENB) test similar to the configurations of the three-point bending test was introduced, as shown in Fig. 5. The model used in three-point bending test was notched at the centre of the bottom by deleting the particles at the notched area. The depth of the notch is half of the height of the specimen. Numerical result for the fracture toughness agreed very well with the experimental measurement for SiC ceramics.[35]

Through abovementioned tests, the macroscopic mechanical properties of polycrystalline SiC assembly in PFC2D were obtained from numerical tests and compared with the experimental results, results are listed in Table 1. As the numerical results agreed with experimental measurements, it was concluded that the SiC assembly constructed in PFC2D could realistically represent for the mechanical behavior of a polycrystalline ceramic element. Therefore, the BPM parameters at particle scale used for the above numerical tests, which was listed in Table 2, could be introduced in the subsequent DEM modeling of cutting process of ceramics.

4. DEM modeling of scratching test

4.1. DEM simulation of the scratching test

The PFC2D has been utilized in this research to develop a DEM model for the simulation of the scratching test of ceramics, using parameters calibrated in Section 3. The dimension of the work piece used for simulation was 0.8 mm in length 0.2 mm in height, and consisted of 5656 particles. There was no friction between the work piece and the lateral and bottom walls. The scratching tool was simplified as a curve with 120° conical angle and a tip radius of 200 μm. The friction factor between the tool and the specimen was set as 0.17, according to the later scratching test results. The scratching speed is 0.05 m/s which was very low to keep the system in quasi-static condition and the scratching depth was 5 μm. An example of the scratching test modeled by DEM has been graphically displayed in Fig. 6. As the scratching tool moved forward, micro-cracks appeared along the trajectory of cutting indicated by red dots in Fig. 6. Because PFC2D is designed for planar problems, it can only describe the vertical cracks. The cracks propagated along the particles' contacts forming tortuous crack paths. The analysis of scratching force vs. the crack numbers is shown in Fig. 7. It can be found in Fig. 7 that the total crack numbers and both the forces in *X* (Fx) and *Y* (Fy) directions increase with the cutting time. There are some spines in both the *X*-force and the *Y*-force curves, and the number of the cracks increased rapidly at the spines which indicate that the initiation of new cracks needs larger forces.

Table 2
DEM parameters for polycrystalline SiC ceramic

Particles	Parallel bonds
$\rho = 3132\,\text{kg/m}^3$	
$R_{max}/R_{min} = 1.5$, $R_{min} = 2.2\,\mu\text{m}$	$\bar{\lambda} = 1.0$
$E_c = 275\,\text{GPa}$	$\overline{E_c} = 275\,\text{GPa}$
$k_n/k_s = 1.1$	$\overline{k_n}/\overline{k_s} = 1.1$
$\mu = 0.5$	$\overline{\sigma_n} = 120 \pm 12\,\text{GPa}$, $\overline{\sigma_s} = 960 \pm 96\,\text{GPa}$

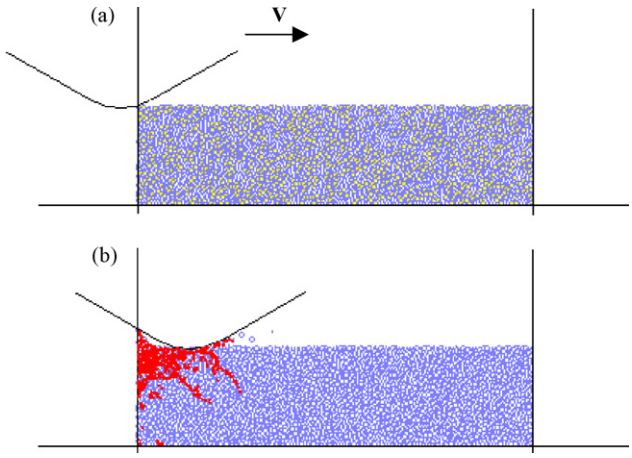

Fig. 6. Simulation of the scratching test. (For interpretation of the references to color in the text, the reader is referred to the web version of the article.)

4.2. Experiment of scratching test

A scratching test, which has been described elsewhere to study the SiC material removal mechanism in wear and machining process,[32–34] was carried out, and results were used in this paper to further validate the developed DEM model for ceramics. The experimental specimen was commercially reactive sinter-

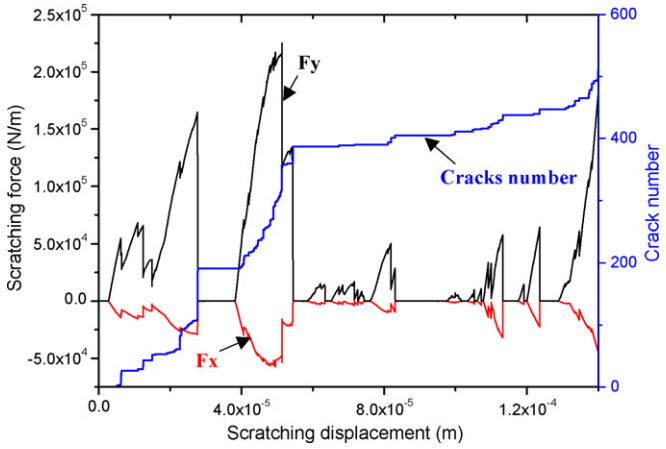

Fig. 7. Scratching force vs. cracks number.

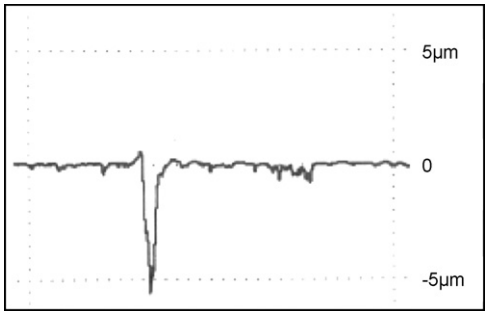

Fig. 8. Profile of the scratching groove.

ing SiC (WeiFang ZhiDa Co., Ltd., China). The scratching test was operated on UMT-2 (CETR, USA). After being polished by nano-diamond in olive oil, and agitated in acetone in an ultrasonic cleaner, the specimen was scratched by a Rockwell diamond indenter with a tip radius of 200 μm and a 120° apex angle, under 20 N constant normal load (Fz), room temperature and without lubricant. The scratching speed was 1 mm/min and the scratching length is 5 mm. The resulting scratching depth was about 5 μm which is the same as the DEM simulation, as shown in Fig. 8 (Mahr S2, Germany). Acoustic emission (AE) also has been used in the experiments to detect the fracture behavior. The data from the scratching test is presented in Fig. 9, and it can be found that the AE signal changes very sharply when the tangential force (Fx) zoomed or precipitated, this coincides with the fracturing events within the sample. Comparing to the numerical results which is shown in Fig. 7, the observations from the scratch test agreed with the DEM simulations qualitatively in terms of the detection of the fracturing in the ceramic specimen.

After scratching, the specimen were polished again with an assistant of an optical microscope (Nikon, USA) until about half width of the scratching groove being removed to enable a SEM (JSM6360, Japan) view of the subsurface right under the scratching groove and parallel to the scratching direction. As illustrated in Fig. 10a, there are many mciro-cracks accumulating under the scratching groove, where material has been heavily damaged and will easily be removed in the subsequent machining process. Some of the micro-cracks propagated into the bulk material and forming a macro-crack, leading to a subsurface damage (Fig. 10b). These observed crack propagation and damage behaviors from the scratching test are very similar

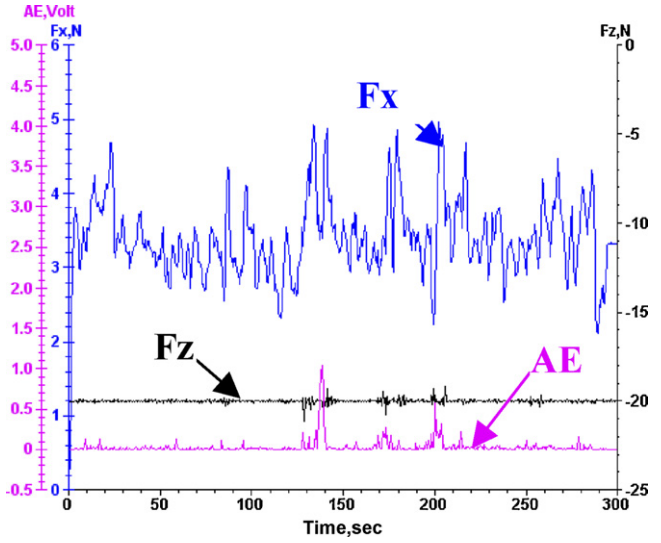

Fig. 9. Scratching test of polycrystalline SiC with AE.

to those obtained from DEM simulation results, as can be seen in Fig. 6.

5. DEM modeling of micro-cracks and damage in machining process

Recently, DEM was applied to simulate cutting process of rock.[27,30] Though rock and ceramics are both brittle materials, the focus of the machining methods for them is quite different. The civil engineers concerned more about the probability and difficulty of the cutting process, while researchers working in the area of the ceramics machining paid more attention to the precision and quality of the machining process. Hence, there are just a few attempts to model the microscopic material and mechanical behavior of ceramics during the machining process using DEM.[36]

After being validated by comparing the results of the DEM simulation and the scratching experiment, DEM then was used to simulate the SiC cutting process. The DEM model for simulation of the cutting process of ceramics was similar to the model in Section 4 except the geometry of the cutting tool. A rigid two-double wall was formed to act as a cutting tool, and ploughed into the work piece and moved with various assigned velocities to simulate the cutting process of the ceramic work piece. The

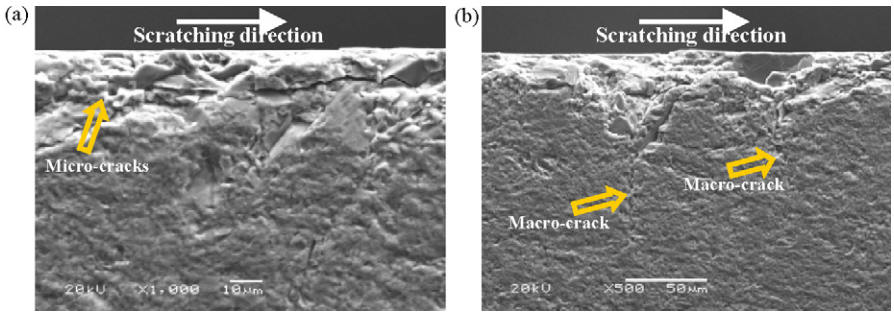

Fig. 10. SEM images of the longitude section of the scratching groove. (a) Micro-cracks accumulated under the scratching groove. (b) Macro-cracks propagated into the subsurface.

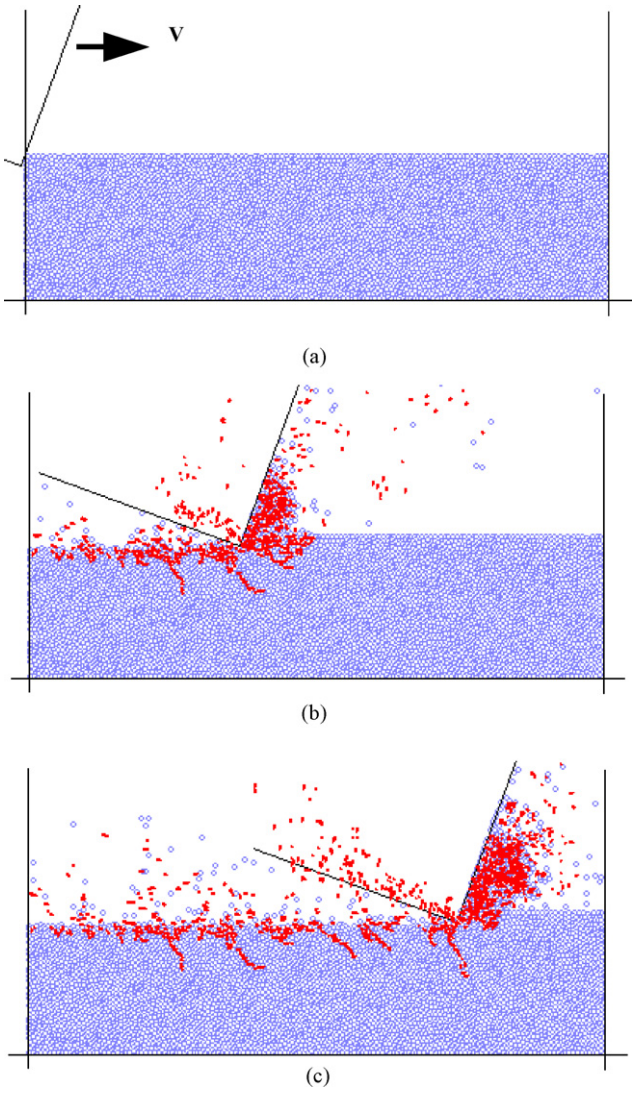

Fig. 11. Simulation of the cutting process.

total cutting distance was 0.6 mm. Through changing the cutting speed v, the rake angle of the cutting tool γ, and the cutting depth a_p, the propagation of micro-cracks and the damage on the finished surfaces can be observed and evaluated under different cutting conditions. An example of the cutting process modeled by DEM has been graphically displayed in Fig. 11, with $v = 5$, $a_p = 15$ μm. As the cutting tool moved forward, there were more and more dispersed or still bonded particles accumulated in front of the cutting tool in Fig. 11. There were also some cracks propagating forward and leading to the removal of the front material. In order to estimate the effects of the cutting speed and the cutting depth on the crack damage to the finished surfaces, three different cutting speeds ($v = 5$ m/s, 10 m/s, and 15 m/s) and six different cutting depths ($a_p = 2$ μm, 5 μm, 10 μm, 15 μm, 20 μm, and 25 μm) were simulated in PFC2D. Every case has been repeated five times in DEM simulation with different random generating seeds in PFC2D so that the random effect of packing can be eliminated. An average result from five runs was used in the later result analysis. The results of total crack numbers and crack maximum depth underneath the finished surface

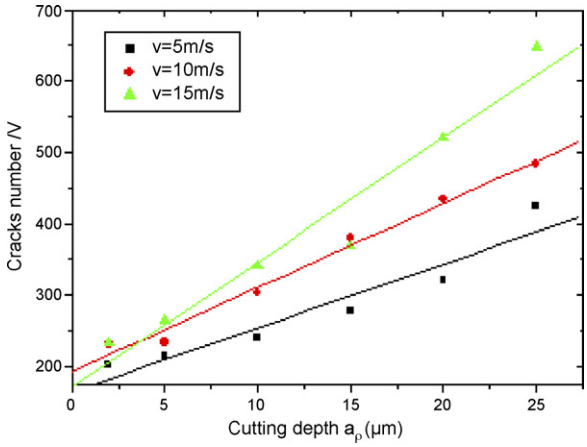

Fig. 12. Total cracks number beneath the finished surface.

were presented against different cutting speeds, depths and cutting angles in Figs. 12 and 13. The inelastic zone which was analyzed in Ref. [31] has also been observed and supported by the numerical results, as illustrated in Figs. 14–17. Numerical results are further analyzed in Section 6 of this paper.

6. Results and discussion

6.1. Crack damage analysis

The cracks number and the maximum crack depth on the machined surface were used as critical quantities for the investigation of the damage caused by micro-cracks; corresponding numerical results are presented in Figs. 12 and 13. A general trend can be identified in Fig. 12 that the faster the cutting tool goes into the work piece, the more cracks beneath the finished surface can be found; the crack number also increases with the cutting depth, and the lower the cutting depth, the less effects of the cutting speed on the cracks number. It is not difficult to see in Fig. 13 that under a faster cutting speed, the maximum depth of cracks increases quicker with the cutting depth. Combining Fig. 12 with Fig. 13, it can be concluded that when cutting speed is higher, the effects of the cutting depth on the quality of the

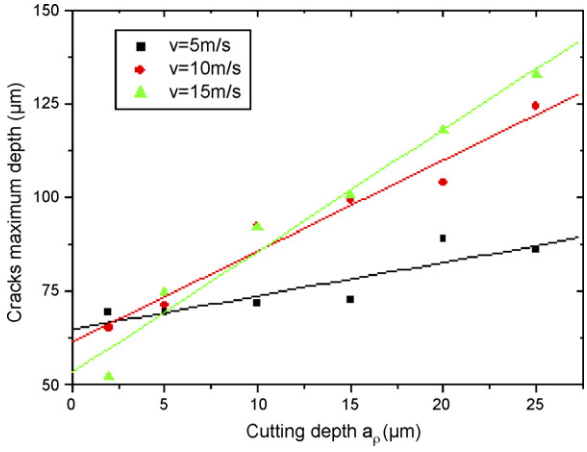

Fig. 13. Maximum depth of cracks beneath the finished surface.

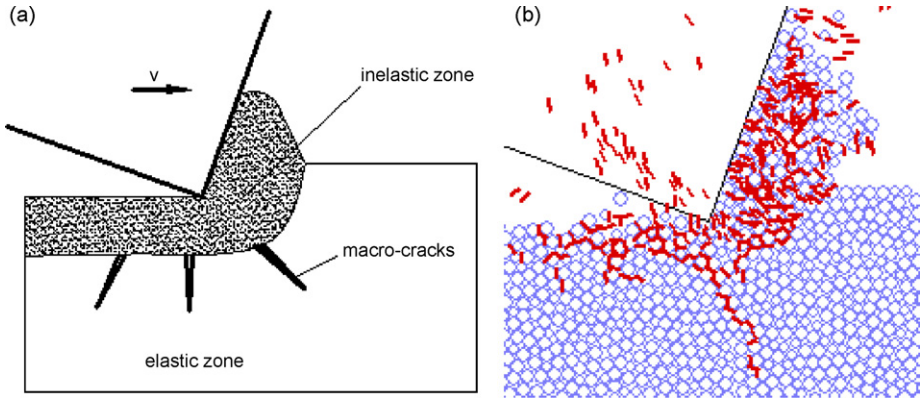

Fig. 14. (a) Micro-cracks and macro-crack described in Ref. [31]; (b) DEM simulation in the process of micro-cutting.

finished surface become more significant. Based on the findings from DEM modeling, lower cutting depth should be combined with higher cutting speed so that the damage to the finished surface can be reduced, and optimal results of machining can be achieved.

6.2. Inelastic zone

According to the theory proposed in Ref. [31] as demonstrated in Fig. 14a, the material under the cutting tool can be divided into two different zones, the inelastic zone and the elastic zone. In the inelastic zone, there are a number of micro-cracks, some of which may propagate through the inelastic zone and formed macro-cracks in the elastic zone. Similar phenomena can be observed in DEM simulation, as is shown in Fig. 14b. In order to estimate the depth of the inelastic zone, the results of the simulations were plotted in terms of accumulated crack numbers vs. depth beneath the finished surface. A typical cutting speed ($v = 10$ m/s) and cutting depth ($a_p = 15$ μm) were chosen as a representative case, and results are presented in Figs. 15 and 16. It can be found in both figures that the crack numbers firstly increase linearly with the depth beneath the finished surface, then show a trend of slower increase below a certain depth, and eventually turn into a steady number represented by the horizontal segments in the data lines. A sketch is generalized from the numerical results to analyze the problem more schematically, as shown in Fig. 17. Section OA can be regarded as the

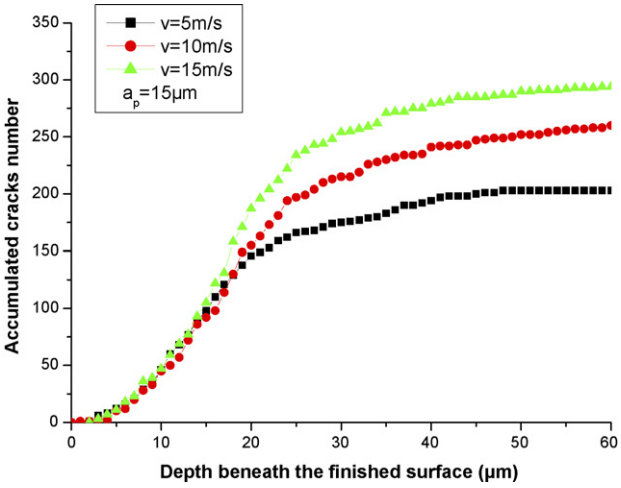

Fig. 16. Accumulated cracks number vs. depth beneath the finished surface ($a_p = 15$ μm, $v = 5$ m/s, 10 m/s, and 15 m/s).

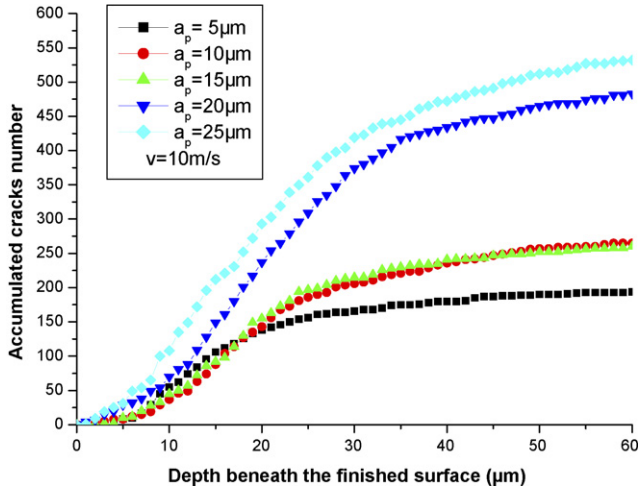

Fig. 15. Accumulated cracks number vs. depth beneath the finished surface ($v = 10$ m/s, $a_p = 5$ μm, 10 μm, 15 μm, 20 μm, and 25 μm).

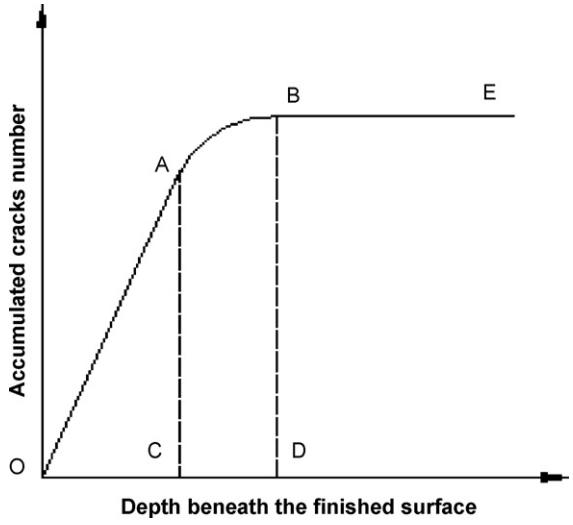

Fig. 17. A sketch of cracks number vs. depth beneath the finished surface.

representation of the numbers of micro-cracks in inelastic zone, whereas AB represents for the number of micro-cracks in a transient elastic zone and BE represents for a completed elastic zone without any damages. The coordinate value of point C can be taken as the depth of the inelastic zone. The distance between C and D can be regarded as the average length of macro-cracks. The generalization process demonstrated in Fig. 17 was applied to analyze the numerical results presented in Figs. 15 and 16. As can be see in Fig. 15, under cutting speed $v = 10$ m/s, the depth of inelastic zone increased with the cutting depth; as for a fixed cutting depth $a_p = 15$ μm in Fig. 16, higher cutting speed would lead to deeper inelastic zone. The effects of cutting speed and cutting depth on the length of the macro-cracks can also been observed in Fig. 13.

7. Conclusions

The discrete element model for polycrystalline SiC ceramics has been developed to study the machining process of ceramics. Microscopic material properties for particles and contacts were calibrated by comparing the results of numerical experiments such as unconfined compressive test, Brazilian test, three-point bending test and fracture toughness test with the equivalent experimental results. The numerical results showed that DEM is a suitable approach to simulate the mechanical behaviors of ceramics. The machining process of SiC ceramics under different cutting conditions has been simulated by the developed DEM model using the calibrated properties for microscopic particles. Numerical results have clearly demonstrated rational trends of the correlations between microscopic damage on the finished surface and the cutting conditions. DEM model has also been validated against the observations from scratch test and SEM pictures. The inelastic zone beneath the finished surface has been identified and quantified by DEM simulations, and range of such a zone can be defined through the analysis of the numerical results. The capability of DEM in the simulation of the ceramics micro-cutting process has been confirmed by this study, and further applications of DEM will focus on three-dimensional simulations and more quantitative investigations on the ceramic machining process.

Acknowledgements

This work was supported by the National Natural Science Foundation of China (50675185) and by the program of New Century Excellent Talents (NCET06-0708).

References

1. Kitajima, K., Cai, G. Q. and Kumagai, N., Study on mechanism of ceramics grinding. *Annals of the CIRP*, 1992, **41**, 367–371.
2. Huang, H. and Liu, Y. C., Experimental investigations of machining characteristics and removal mechanisms of advanced ceramics in high speed deep grinding. *International Journal of Machine Tools & Manufacture*, 2003, **43**, 811–823.
3. Desa, O. and Bahadur, S., Material removal and subsurface damage studies in dry and lubricated single-point scratch tests on alumina and silicon nitride. *Wear*, 1999, **225–229**, 1264–1275.
4. Wataru, K., Subsurface damage in scratch testing of silicon nitride. *Wear*, 2004, **256**, 100–107.
5. Patten, J. A., Gao, W. and Yasuto, K., Ductile regime nanomachining of single-crystal silicon carbide. *ASME Journal of Manufacturing Science and Engineering*, 2005, **127**(8), 522–532.
6. Jasinevicius, R. G., Influence of cutting conditions scaling in the machining of semiconductors crystals with single point diamond tool. *Journal of Materials Processing Technology*, 2006, **179**, 111–116.
7. Lawn, B. R., Evans, A. A. and Marshall, I. B., Elastic/plastic indentation damage in ceramics: the median/radial crack system. *Journal of the American Ceramic Society*, 1980, **63**, 574–578.
8. Zhang, B. and Peng, X. H., Grinding damage prediction for ceramics via CDM model, Journal of Manufacturing Science and Engineering. *Transactions of the ASME*, 2000, **122**, 51–58.
9. Chuang, T. J., Jahanmir, S. and Tang, H. C., Finite element simulation of straight plunge grinding for advanced ceramics. *Journal of the European Ceramic Society*, 2003, **23**, 1723–1733.
10. Pei, Q. X., Lu, C., Fang, F. Z. and Wu, H., Nanometric cutting of copper: a molecular dynamics study. *Computational Materials Science*, 2006, **37**(4), 434–441.
11. Patten J. A., *High pressure phase transformation analysis and molecular dynamics simulations of single point diamond turning of germanium*, PhD Dissertation, NCSU, 1996.
12. Han, X. S., Study micromechanism of surface planarization in the polishing technology using numerical simulation method. *Applied Surface Science*, 2007, **253**(14), 6211–6216.
13. Cai, M. B., Li, X. P. and Rahman, M., Study of the mechanism of nanoscale ductile mode cutting of silicon using molecular dynamics simulation. *International Journal of Machine Tools & Manufacture*, 2007, **47**, 75–80.
14. Brook, J. R., *Processing of Ceramics. Part II. Materials Science and Technology, vol. 17B*. Federal Republic of Germany, Weinheim, 1996.
15. Holt, R. M., Kjølaas, J., Larsen, I., Li, L., Gotusso Pillitteri, A. and Sønstebøø, E. F., Comparison between controlled laboratory experiments and discrete particle simulations of the mechanical behavior of rock. *International Journal of Rock Mechanics & Science*, 2005, **42**, 985–995.
16. Fakhimi, A., Carvalho, F., Ishida, T. and Labuz, J. F., Simulation of failure around a circular opening in rock. *International Journal of Rock Mechanics & Science*, 2002, **39**, 507–515.
17. Zhang, R. and Li, J. Q., Simulation on mechanical behavior of cohesive soil by discrete element method. *Journal of Terramechanics*, 2006, **43**, 303–316.
18. Sheng, Y., Lawrence, C. J., Briscoe, B. and Thornton, C., Numerical studies of uniaxial powder compaction process by 3D DEM. *Engineering Computations: International Journal for Computer-Aided Engineering*, 2004, **21**(2–3), 304–317.
19. Cundall, P. A. and Strack, O. D. L., A discrete mumerical model for granular assemblies. *Géotechnique*, 1979, **29**(1), 47–65.
20. Hunt, S. P., Meyers, A. G. and Louchnikov, V., Modelling the Kaiser effect and deformation rate analysis in sandstone using the discrete element method. *Computers and Geotechnics*, 2006, **30**, 611–621.
21. Lobo-Guerrero, S. and Vallejo, L. E., DEM analysis of crushing around driven piles in granular materials. *Géotechnique*, 2005, **55**(8), 617–623.
22. Frédéric, S. H., Donzé, V. and Daudeville, L., Discrete element modeling of concrete submitted to dynamic loading at high strain rates. *Computers & Structures*, 2004, **82**, 2509–2524.
23. Itasca Consulting Group Inc., *Particle Flow Code in 2-Dimensions (PFC2D)*, Version 3.10, Minneapolis, Minnesota, 2004.
24. Potyondy, D. O. and Cundall, P. A., A bonded-particle model for rock. *International Journal of Rock Mechanics & Mining Science*, 2004, **41**, 1329–1364.
25. Potyondy, D. O., Simulating stress corrosion with a bonded-particle model for rock. *International Journal of Rock Mechanics & Mining Science*, 2007, **44**, 677–691.
26. Itasca Consulting Group Inc., *PFC2D User's Manuals*, 2004.
27. Huang, H., *Discrete Element Modeling of Tool–Rock Interaction*, PhD Dissertation, University of Minnesota, 1999.
28. Yu, R. C., Ruiz, G. and Pandolfi, A., Numerical investigation on the dynamic behavior of advanced ceramics. *Engineering Fracture Mechanics*, 2004, **71**, 897–911.

29. Bažant, Z. and Chen, E. P., Scaling of structural failure. *Applied Mechanics Review*, 1997, **50**(10), 593–627.
30. http://www.itascacg.com/pfc_ex_rockcut.html.
31. Zhang, B., Tokura, H. and Yoshikawa, M., Study on surface cracking of alumina scratched by single-point diamonds. *Journal of Materials Science*, 1988, **23**, 3214–3224.
32. Axén, N., Kahlman, L. and Hutchings, I. M., Correlations between tangential force and damage mechanisms in the scratch testing of ceramics. *Tribology International*, 1997, **30**(7), 467–474.
33. Bhattacharya, B., Patten, J. A. and Jacob, J., Ductile to brittle transition depths for CVD silicon carbide and quartz. *International Journal of Machining and Machinability of Materials*, 2007, **2**, 17–36.
34. Subhash, G. and Bandyo, R., A new scratch resistance measure for structural ceramics. *Journal of the American Ceramic Society*, 2005, **88**(4), 918–925.
35. http://www.ceramics.org/cic/propertiesda.asp.
36. Lei, S. and Yang, B., Distinct element simulation of ceramic machining: material removal mechanism. *Transactions of the North American Manufacturing Research Institution of SME*, 2005, **33**, 485–492.